Advances in Science and Technology Research Journal

*Advances in Science and Technology Research Journal*, 2026, 20(2), 94–113
https://doi.org/10.12913/22998624/210743
ISSN 2299-8624, License CC-BY 4.0

Received: 2025.06.23
Accepted: 2025.11.15
Published: 2025.12.23

# Comparison of unsupervised machine learning segmentation algorithms in the analysis of unmanned aerial vehicle – based multispectral crop images

Paweł Karpiński[1*], Jakub Rzeczkowski[2]

[1] Department of Machine Operation and Production Processes Management, Faculty of Production Engineering, University of Life Sciences in Lublin, Głęboka 28, 20-612 Lublin, Poland
[2] Faculty of Mechanical Engineering, Lublin University of Technology, Nadbystrzycka 38d, 20-618 Lublin, Poland
* Corresponding author's e-mail: pawel.karpinski@up.edu.pl

## ABSTRACT

In precision agriculture, the analysis of UAV-based multispectral imagery enables spatial differentiation of crop condition, supporting targeted management decisions. This study compares the performance of two unsupervised segmentation algorithms (K-means and Gaussian Mixture Models) in analyzing RGB images of winter wheat, supported by NDVI-based interpretation. Segmentation was performed on RGB orthomosaics acquired at two phenological stages, followed by NDVI analysis to assign physiological meaning to each segment. The average NDVI per cluster was used to reconstruct NDVI maps and objectively assess vegetation condition within segments. In the early growth stage, segmentation primarily reflected spectral variability in the soil background due to low biomass and weak plant–soil contrast. NDVI analysis revealed that seemingly regular clusters corresponded to bare inter-row soil rather than emerging plants – highlighting the limited diagnostic value of RGB segmentation alone at this stage. In the later growth stage, both algorithms accurately delineated field plots and intra-field variability. Using five clusters, the analysis identified zones ranging from dense, healthy vegetation to bare soil. These results demonstrate that combining RGB-based unsupervised segmentation with NDVI analysis is an effective tool for mapping spatial heterogeneity in mature crops, while offering limited standalone value in early growth stages without additional spectral verification.

**Keywords:** image segmentation, multispectral imagery, K-means clustering, gaussian mixture model (GMM), precision agriculture, drone-based crop monitoring.

## INTRODUCTION

Agriculture plays a strategic role in the economy, and the optimization of agronomic practices alongside the pursuit of sustainable crop production is becoming increasingly important. In recent years, the information revolution has fueled the rapid development of the big data domain, which now serves as one of the primary sources of innovation across numerous sectors. A growing number of organizations regard large datasets as the backbone of information management infrastructure and as a foundation for decision-support analytics. Data mining techniques enable the extraction of knowledge from databases by identifying patterns that are relevant, novel, potentially useful, and understandable.

In the context of precision agriculture and site-specific management, remotely sensed data play a key role in monitoring crop condition and vegetation dynamics. One of the most widely used indices in remote sensing image analysis is the normalized difference vegetation index (NDVI) [1], which is employed to assess vegetation cover and crop health. Temporal NDVI profiles allow the identification of characteristic vegetation development patterns. Other indices, such as NDRE (normalized difference red edge index)

and OSAVI (optimized soil adjusted vegetation index), are also used to assess crop condition [2].

Traditional methods of crop mapping rely primarily on in-field data collection, which requires recalibration for each new growing season. Meanwhile, yield maps – often promoted as tools for delineating management zones – exhibit significant temporal variability due to changing weather conditions, agronomic practices, pathogen pressure, and pest presence. The application of clustering methods to remote sensing data – especially to temporal NDVI profiles – enables the identification of stable, homogeneous zones within agricultural fields that reflect actual crop growth conditions. Remote data can be acquired using drones [3] or satellites [4].

One of the key challenges associated with remotely sensed imagery used for crop monitoring is the presence of missing data. An effective approach to addressing this issue involves the reconstruction of missing values using gaussian mixture models (GMM) trained with the expectation–maximization (EM) algorithm [5]. This method was employed by Othman et al. [6] for forecasting sugarcane crop infestation patterns. Another application of GMM involves the classification of spectral data acquired by UAVs to develop a rapid and non-destructive method for estimating nitrogen and phosphorus distribution in cotton leaves [7].

Big data analysis in agriculture relies on data mining techniques, whose primary objective is to forecast yields and identify optimal agronomic parameters to maximize production efficiency. To capture the complexity of agricultural data and extract meaningful insights, clustering algorithms are commonly employed. One of the most frequently used is the K-means algorithm, which can also be applied to the analysis of meteorological data [8]. An example of its application is the classification of climate vegetation types based on combined satellite and climate data, such as precipitation and temperature [9]. This approach better reflects the relationships between vegetation and climatic conditions compared to methods using only a single type of data. A comprehensive review of data mining techniques in agriculture is presented in [10], where these methods are divided into two major categories: classification techniques and clustering techniques.

The main challenges associated with the use of the K-means algorithm include selecting the optimal number of clusters (K value) and identifying suitable initial centroids. In the traditional version of the algorithm, cluster centers are selected randomly, which may result in unstable and suboptimal outcomes. Improved results can be achieved through hybrid versions of the algorithm, such as Hybrid K-means [11]. In [12], the authors analyzed dynamic initialization of centroids in a Bayesian gaussian mixture model (BGMM) in the context of orchard crop data. In [13], an improved K-means algorithm was proposed based on the maximum-distance method for determining initial cluster centers. It was shown that, compared to the standard algorithm, the improved method yields better clustering quality and higher computational efficiency.

Data mining techniques applied in agriculture can be categorized into four main groups: association rules, classification, clustering, and regression [14]. Each of these approaches utilizes different algorithms to process data and transform it into useful and interpretable knowledge. The most commonly used methods include K-means, K-nearest neighbors (KNN), artificial neural networks (ANN), and support vector machines (SVM) [15]. Other algorithms include partitioning around medoids (PAM), clustering large applications (CLARA), modified density-based spatial clustering of applications with noise (DBSCAN), and multiple linear regression (MLR) [16][17]. Decision tree, random forest, and XGBoost are also widely used. Notably, Kernel K-means can be integrated with SVM, forming a powerful tool for data classification in the context of precision agriculture [18].

In smart farming systems, large volumes of data are generated by various sources, including sensors operating within the internet of things (IoT) framework. In [19], sixteen data reduction techniques were analyzed, testing combinations of eight machine learning methods, including K-means and GMM. The study found that the most effective data reduction was achieved by combining the K-means algorithm with run-length encoding (RLE) compression.

Clustering algorithms are widely used for plant recognition in natural field conditions. However, their effectiveness heavily depends on environmental factors such as lighting, as well as on the degree of color similarity between weeds and crop plants. A low-cost, real-time solution for plant recognition in natural environments involves combining Binocular Stereo Vision technology with clustering based on a GMM [20]. Kim et al. [21] applied the GMM algorithm to analyze the

individual mass distribution of triticale grains, and this approach can also be extended to assess other morphological characteristics of plants.

An improved version of the K-means algorithm with an adaptive number of clusters, designed for segmenting tomato leaf images, was presented in [22]. Meanwhile, [23] introduced a weighted K-means clustering algorithm that uses multiple image features to segment fruit images. To distinguish between crops and weeds, one may use semantic segmentation based on deep learning, utilizing the subtractive clustering algorithm [24], or an approach based on convolutional neural networks (CNN) [25]. In this context, the K-means algorithm can play a key role in unsupervised feature learning as a pre-training step for the CNN model.

Semi-supervised segmentation using GMM has been successfully applied for the automatic detection of invasive plant flowers [26]. This approach reduces the dependence on large, manually annotated datasets, offering an advantage over deep learning methods that require full data annotation. Additionally, a combination of CNN with the K-means clustering algorithm for grouping NDVI data has been used to assess plant health in a vineyard [27]. The results of that study showed that processed NDVI maps obtained after clustering better reflected crop conditions than raw satellite data.

One of the key applications of clustering algorithms is the assessment of plant health. Leaf disease detection and classification can be carried out using the extreme learning machine (ELM) deep learning algorithm, based on real-world image datasets. Infected leaf areas can be extracted using the K-means clustering algorithm [28]. In [29], an image processing system was presented for detecting two major turmeric leaf diseases: Leaf spot and leaf blotch. The K-means Segmentation algorithm was used to segment diseased leaf regions, while the SVM classifier was employed to identify specific diseases.

Another important area of classification algorithm application in agriculture is the identification of management zones. The goal of this analysis is to divide a field into sub-areas with different characteristics, enabling the implementation of site-specific management strategies. Management zones can be defined based on various input data such as yield, soil properties, or vegetation indices. K-means and Fuzzy C-means algorithms can be applied to analyze NDVI maps generated from satellite imagery to extract these zones [30]. An innovative method for delineating management zones in maize cultivation, based on the NDVI index and an improved SOM-K-means algorithm, was proposed in [31]. Nugumanova et al. [32] compared four different clustering algorithms for defining homogeneous management zones. Gavioli et al. [33] conducted a comprehensive comparative analysis involving 20 different clustering algorithms, evaluating their usefulness in delineating management zones. In [34], the influence of input data type and feature selection methods on the quality of zone delineation was investigated using five different clustering algorithms. Johann et al. [35] compared the performance of the K-means, MAXVER, and DBSCAN algorithms in the context of management zone segmentation in soybean cultivation.

There are numerous examples of classification algorithms applied to land mapping. The K-means algorithm can be used for the classification and quantitative assessment of land cover affected by floods [36] or landslides [37]. Mapping of waterlogged crops can also be performed using satellite data with an unsupervised GMM [38]. Sanz et al. [39] applied the K-means algorithm in combination with the unsupervised random forest (URF) method to cluster arid grazing lands. The best results were obtained when URF was combined with the Hurst exponent, calculated using the Detrended Fluctuation Analysis (DFA – $H_2$) method.

Land mapping using the K-means algorithm and satellite-derived NDVI data can be performed within programming environments such as MATLAB, Python, or R. It may provide an alternative to traditional GIS software [40]. The topic of mapping winter crops over large areas was addressed in [41], where a GMM model was employed to automatically distinguish such crops from others by modeling the distribution of a phenological index derived from NDVI. An original approach to soybean crop mapping was presented in [42], which introduced a spectral gaussian mixture model (SGMM) using Bhattacharyya coefficient weighting to optimize the probabilistic spectral separability between soybean and other crops.

Crop mapping may also involve yield analysis and estimation. The algorithm proposed in [43] enabled the classification of NDVI data obtained from both satellite and UAV sources for paddy rice crops, as well as the identification of factors influencing high productivity. NDVI data

can also be collected using handheld optical sensors. A clustering analysis of winter wheat using this method showed that the agreement between yield classes and NDVI-based classes was higher under dryland farming conditions [44]. Another example includes the use of data from a soil plant analyzer development (SPAD) chlorophyll meter combined with imagery from a spectral camera mounted on an UAV [45].

A synergistic integration of the supervised Random Forest algorithm with the unsupervised K-means clustering algorithm enables the development of crop recommendation strategies tailored to specific soil and weather conditions [46]. Soil condition analysis can be conducted using the Parallel K-means algorithm, which provides higher efficiency and accuracy compared to classical and analytical variants [47]. The identification of key soil and topographic features necessary for delineating potential management zones was demonstrated in [48].

Alternative clustering methods, such as hierarchical algorithms or density-based approaches (e.g., DBSCAN), have also been applied in remote sensing and agricultural image analysis. However, these techniques often face challenges when dealing with large-scale UAV orthomosaics, including high computational cost, sensitivity to parameter selection, and difficulties in handling continuous spectral gradients. In contrast, K-means and gaussian mixture models represent well-established, computationally feasible, and widely validated methods in the literature, frequently serving as benchmarks in segmentation studies. For this reason, the present work focuses on K-means and GMM as representative and complementary approaches, providing algorithmic efficiency.

In summary, clustering combined with remote sensing indices has a wide range of applications in various domains related to agriculture and environmental protection. Clustering methods are also widely applied in other scientific fields, including medicine [49], manufacturing industry [50], and materials strength analysis [51]. The conducted literature review revealed that these techniques can be used for tasks such as image segmentation (e.g., of plant leaves, crop surfaces, flooded areas), identification of homogeneous regions, mapping of management zones in precision agriculture, and monitoring vegetation condition and hydrological phenomena. The K-means clustering algorithm also finds less obvious applications, such as in the analysis of precision marketing strategies in the agricultural sector [52]. Clustering methods rely on both satellite data and imagery acquired from cameras mounted on UAVs. In this context, optimization of algorithms and integration of data from various sources are of key importance.

Despite numerous studies comparing the effectiveness of satellite and aerial image segmentation methods, there is still a lack of research focusing solely on drone-derived data, which are characterized by significantly higher spatial resolution and high temporal variability. UAV-acquired imagery requires appropriate adaptation of analytical methods, considering local lighting conditions, potential georeferencing errors, and disturbances resulting from the motion of the measurement platform. In light of these considerations, the present study addresses this gap by focusing on the unique aspect of comparing the effectiveness of two unsupervised segmentation algorithms – K-means and the GMM – in the analysis of multispectral drone imagery of crop fields. The analysis was conducted using data acquired with an unmanned aerial vehicle.

The following section of the article presents the details of the applied methodology and the adopted approach to image analysis, including source data and algorithms used. Subsequently, the obtained results are presented and discussed. The article concludes with a summary of the findings and recommendations for future research directions.

## METHODOLOGY

### Drone and mission parameters

To acquire imagery for further mathematical analysis, two flights were conducted using the DJI Mavic 3M unmanned aerial vehicle (Figure 1). The drone is equipped with a multispectral camera consisting of four lenses, and a separate RGB camera. The multispectral sensor captures the following spectral bands: near-infrared (NIR), red edge, red, and green, each at a resolution of 5 MP. The RGB camera captures visible spectrum images at a resolution of 20 MP. The bandwidth for the green, red, and red edge bands was 32 nm, and for the NIR band it was 52 nm. The central wavelengths of the respective bands were: 560 nm (green), 650 nm (red), 730 nm (red edge), and 860 nm (NIR). Selected


(a) (b)

**Figure 1.** (a) Drone used for research and (b) multispectral camera on a drone: 1 – near-infrared lens; 2 – red edge band lens; 3 – red band lens; 4 – green band lens; 5 – RGB lens

technical parameters of the imaging system are summarized in Table 1.

The flights were performed in 2025 at the Czesławice Experimental Farm, operated by the University of Life Sciences in Lublin, Poland. The first flight took place on 28 March, and the second on 22 May, corresponding to the phenological stages BBCH 29 (tillering) and BBCH 55 (heading), respectively. These stages were chosen due to significant changes in biomass/leaves, which effectively differentiate the NDVI. The UAV operated with onboard RTK (real time kinematic) module enabled, ensuring high geolocation accuracy during image acquisition and facilitating accurate georeferencing of the orthomosaic. Weather conditions during both flights were clear, with minimal wind and consistent sunlight, ensuring stable image acquisition.

Flight paths were executed based on predefined mission parameters, as outlined in Table 2. The monitored area had a rectangular shape and a total surface of 1.03 hectares. The UAV flew along a programmed grid pattern at an altitude of 40 meters above ground level, which allowed for the acquisition of imagery with a high GSD of 1.85 cm/pixel. The flight was conducted in AGL (above ground level) mode with real-time follow and elevation optimization functions enabled. To ensure high-quality orthomosaic generation, overlapping parameters were set to 80% frontal and 70% side overlap.

**Table 1.** Selected technical parameters of the camera

| Parameter | Value/Description |
|---|---|
| Multispectral camera | |
| Resolution | 5 MP (2592 × 1944 px) |
| Field of view | 73.91° |
| Equivalent focal length | 25 mm |
| Aperture | f/2.0 |
| Shutter speed | Electronic shutter: 1/30–1/12800 s |
| RGB camera | |
| Resolution | 20 MP (5280 × 3956 px) |
| Field of view | 84° |
| Equivalent focal length | 24 mm |
| Aperture | f/2.8 to f/11 |
| Shutter speed | Electronic shutter: 8–1/8000 s |

All flights were conducted under clear-sky conditions at comparable times of day to minimize variation in solar elevation. The UAV platform (DJI Mavic 3M) is equipped with an integrated sunlight sensor that continuously measures incident light and applies radiometric correction during image acquisition. This hardware-based calibration ensured that differences between datasets primarily reflected crop growth stage rather than variability in illumination.

Orthomosaic maps and NDVI maps were generated using the DJI SmartFarm Web Tool. The processed images were exported in TIF format and subsequently subjected to mathematical analysis. Due to the very high resolution of the resulting maps, selected subsets of the images with a size of 1200 × 1200 pixels were extracted for detailed analysis. The tile size was selected to ensure both sufficient spatial resolution for pattern identification and efficient computational processing.

The NDVI was calculated according to the standard formula:

$$NDVI = \frac{NIR - RED}{NIR + RED} \quad (1)$$

where: *NIR* – reflectance in the near-infrared range; *RED* – reflectance in the red range.

**Table 2.** Technical parameters of the flight mission

| Parameter | Value/Description |
|---|---|
| Mapping area | 10 301 m² |
| GSD | 1.85 cm/pixel |
| Distance | 802.0 m |
| Estimated duration | 3 min 45 s |
| Photos | 113 |
| Mode | Ortho Collection |
| Altitude mode | AGL |
| Route altitude | 40.0 m |
| Speed | 3.5 m/s |
| Course angle | 338° |
| Side overlap ratio | 70% |
| Frontal overlap ratio | 80% |
| Margin | 0 m |
| Photo mode | Timed Interval Shot |

To emphasize the variability of segmentation performance, two measurement dates were deliberately chosen to represent extreme phenological stages of winter wheat: the early tillering stage (BBCH 29) with minimal biomass and poor vegetation–soil contrast, and the heading stage (BBCH 55) with dense canopy cover and strong spectral separability. This design enabled the evaluation of algorithmic performance under conditions of both limited and pronounced spectral differentiation, providing insight into the realistic applicability of unsupervised clustering in precision agriculture. Subsequent analyses were performed using the unsupervised segmentation algorithms the K-means clustering and the GMM, which are described in detail in the following subsections.

## K-means algorithm

The K-means clustering algorithm constitutes a foundational technique in unsupervised learning and has been widely adopted in image segmentation due to its algorithmic simplicity and computational tractability. In the context of image analysis, segmentation is formulated as a clustering problem, where the objective is to partition the image into semantically or statistically homogeneous regions. Each image element, typically a pixel, is treated as a data point $x_i \in N^d$, and is assigned to one of $K$ clusters based on feature similarity. The method operates by minimizing the total intra-cluster variance, expressed as the following objective function:

$$J = \sum_{k=1}^{K} \sum_{x_i \in C_k} \|x_i - \mu_k\|^2 \tag{2}$$

where $\mu_k$ denotes the centroid of cluster $C_k$, computed as the mean of all feature vectors assigned to that cluster.

The feature vector $x_i$ may include pixel intensity values, color components (e.g., RGB), spatial coordinates, or other descriptors such as texture or filter responses, depending on the desired segmentation properties.

The algorithm proceeds through an iterative process composed of two alternating steps:

1. Cluster assignment – each pixel is assigned to the cluster with the nearest centroid, using the Euclidean distance in the selected feature space:

$$c_i = \arg \min_{k \in \{1,\ldots,K\}} \|x_i - \mu_k\|^2 \tag{3}$$

2. Centroid update – the centroid of each cluster is recomputed as the mean of the assigned pixel vectors:

$$\mu_k = \frac{1}{|C_k|} \sum_{x_i \in C_k} x_i \tag{4}$$

These steps are repeated until convergence, typically defined as the stabilization of cluster assignments or a negligible decrease in the objective function. The final cluster labels define the segmentation mask, with each cluster corresponding to a distinct region in the image.

In image segmentation, the K-means is particularly effective when the objects to be segmented differ significantly in color or intensity. However, its performance may degrade in the presence of complex textures, illumination gradients, or overlapping class distributions. Moreover, the algorithm assumes that clusters are convex and isotropic in the feature space, which may not hold in real-world images. The number of clusters $K$ must also be predefined, which can be non-trivial without prior knowledge of the image structure.

To address these limitations, several extensions have been introduced. For example, the K-means improves initialization stability, while spatially-augmented feature spaces incorporate pixel coordinates to encourage regional smoothness. In more advanced settings, the K-means is integrated into multi-stage pipelines alongside graph-based methods, the Markov Random

Fields, or the deep convolutional features to improve accuracy and robustness.

Despite these limitations, the K-means remains a widely used method in image segmentation, valued for its efficiency, interpretability, and ease of implementation. It is frequently used as a baseline or preprocessing step in both classical and deep learning-based image analysis workflows.

## Gaussian mixture model

GMMs are probabilistic clustering techniques frequently used in image segmentation, where the objective is to divide an image into regions with statistically coherent properties. In this technique, each pixel $x_i \in N^d$ is represented as a feature vector encoding its photometric attributes, such as intensity or color components (e.g., RGB), and is assumed to be generated by one of $K$ underlying Gaussian distributions. The overall data distribution is modeled as a weighted sum of these Gaussian components:

$$p(x_i \mid \Theta) = \sum_{k=1}^{K} \pi_k \mathcal{N}\left(x_i \mid \mu_k, \sum k\right) \quad (5)$$

where: $\pi_k$ denotes the mixture weight of component $k$, such that $\Sigma^K_{k=1}\pi_k = 1$, $\mu_k \in \mathbb{R}^d$ is the mean vector, and $\Sigma k \in \mathbb{R}^{d\times d}$ is the covariance matrix. The parameter set $\Theta = \{\pi_k, \mu_k, \Sigma k\}^K_{k=1}$ is optimized via the expectation-maximization (EM) algorithm, which iteratively improves the model fit to maximize the likelihood of the observed image data.

The EM algorithm alternates between two computational steps. In the expectation step (E-step), the posterior probability that a given pixel $x_i$ belongs to cluster $k$ is computed as:

$$\gamma_{ik} = \frac{\pi_k \mathcal{N}(x_i \mid \mu_k, \sum k)}{\sum_{j=1}^{K} \pi_j \mathcal{N}\left(x_i \mid \mu_j, \sum j\right)} \quad (6)$$

where: $\gamma_{ik}$ is referred to as the responsibility of component $k$ for pixel $x_i$. These responsibilities are then used in the maximization step (M-step) to update the model parameters as follows:

$$\pi_k = \frac{1}{n}\sum_{i=1}^{n} \gamma_{ik} \quad (7)$$

$$\mu_k = \frac{\sum_{i=1}^{n} \gamma_{ik}\, x_i}{\sum_{i=1}^{n} \gamma_{ik}} \quad (8)$$

$$\sum k = \frac{\sum_{i=1}^{n} \gamma_{ik}\,(x_i - \mu_k)(x_i - \mu_k)^T}{\sum_{i=1}^{n} \gamma_{ik}} \quad (9)$$

These two steps are repeated until convergence, which is typically defined by the change in log-likelihood falling below a set threshold. Upon convergence, each pixel is assigned to the component with the highest posterior probability $y_{ik}$, resulting in a segmented image where each region corresponds to one of the $K$ Gaussian components.

Unlike K-means, which performs hard assignment and assumes spherical clusters with equal variance, the GMM allows for ellipsoidal clusters with distinct covariance structures and models pixel assignments probabilistically. This flexibility enables it to more accurately capture complex photometric distributions, such as overlapping color regions or subtle gradations in intensity, which are common in real-world images. Moreover, the use of full covariance matrices permits the identification of anisotropic structures that cannot be segmented properly by simpler distance-based methods.

However, the GMM segmentation also introduces certain computational and numerical challenges. The estimation of full covariance matrices can become unstable in high-dimensional feature spaces or when the number of training samples per component is small. Additionally, the EM algorithm may converge to local maxima of the likelihood function, making the initialization step critical to segmentation quality. Despite these challenges, the gaussian mixture models remain a well-established method for unsupervised segmentation, particularly when the underlying class distributions exhibit significant overlap or when a probabilistic representation of uncertainty is desired at object boundaries.

## Adopted research approach

In this study, a multispectral image segmentation approach was employed to analyze vegetation characteristics by using unsupervised machine learning techniques. The methodology involved processing a pair of aligned images: a standard RGB image and a corresponding NDVI map derived from multispectral data. The objective was to segment the RGB image into visually homogeneous regions and evaluate how well

these segments corresponded to the spatial variation in NDVI values.

The RGB images were used in their original BGR color space. Pixel values were reshaped into a two-dimensional matrix, where each row represented an individual pixel with three color channels. The NDVI images, originally represented as an 8-bit grayscale images, were transformed into a floating-point format and normalized to the range from –1 to 1 to preserve its ecological interpretability. Importantly, the NDVI data were not included in the clustering process itself but were used post hoc to characterize the resulting segments.

Two clustering algorithms were applied independently to the RGB pixel data: the K-means clustering and the GMM. For both approaches, the number of clusters was predefined, and a comparative analysis was conducted by varying the number of clusters from 2 to 20. This enabled systematic evaluation of segmentation quality and NDVI reconstruction performance as a function of cluster resolution. In the case of GMM, the covariance structure was set to a diagonal form to allow for variable scaling across features while maintaining computational tractability. Each algorithm assigned a cluster label to every pixel, producing a segmented image where each segment represented a distinct class of visual similarity. For the K-means algorithm, the k-means++ initialization procedure was applied to ensure stable and reproducible centroid selection, thereby reducing sensitivity to random starting conditions. In the case of the Gaussian Mixture Model, initialization was performed using K-means-based estimates of component means, with diagonal covariance matrices derived from the corresponding clusters. This strategy facilitated faster convergence of the expectation–maximization algorithm and improved reliability of the segmentation results. All clustering experiments were executed with a fixed random state parameter to ensure deterministic behavior and full reproducibility of the results. Under these conditions, repeated runs produced identical outcomes, eliminating the need for multiple independent trials or variance analysis. For the K-means algorithm, the maximum number of iterations was set to 300 with a convergence tolerance (epsilon) of $1 \times 10^{-4}$, while for the gaussian mixture model, the expectation-maximization procedure was limited to 1000 iterations with a tolerance of $1 \times 10^{-3}$. These settings reflect standard practice in scikit-learn and were chosen to balance computational efficiency with stable convergence.

Following segmentation, the NDVI map was used to compute the average NDVI value within each cluster. These values were then propagated back to all pixels within their respective segments to construct a reconstructed NDVI image based on clustering structure. This reconstructed map approximated the original NDVI by assigning region-level means, effectively smoothing local variations. To evaluate the correspondence between the original and reconstructed NDVI distributions, standard statistical metrics were computed, including the mean absolute error (MAE), the mean squared error (MSE), and the coefficient of determination ($R^2$). Additionally, an absolute error map was generated to visualize local discrepancies across the spatial domain. The complete computational time required for segmentation and analysis was also recorded to assess the efficiency of the method.

In parallel, cluster-wise statistical summaries were generated to further characterize the segmentation output. For each cluster, the proportion of pixels assigned to that segment (as a percentage of the total image) and the corresponding mean NDVI value were calculated. These statistics provided insight into the relative dominance and vegetation health of each cluster.

Moreover, histogram-based analyses of NDVI distributions were performed on the original NDVI maps. These histograms allowed for visual comparison of pixel-level NDVI frequency distributions, supporting interpretation of the smoothing effect introduced by the region-based averaging.

All analyses were carried out in the Python 3.13.2 programming environment. Image processing and array operations were performed using the OpenCV 4.10.0 and NumPy 2.2.5 libraries. Clustering algorithms were implemented with scikit-learn, which provided tools for the K-means segmentation, Gaussian Mixture Models, and evaluation metrics such as mean absolute error, mean squared error, and the coefficient of determination. Data visualization, including segmentation maps, error maps, and histograms, was conducted using Matplotlib, while data tables and summary statistics were handled with pandas.

The computational experiments were executed on a mobile workstation – a Lenovo ThinkPad T14s Gen 2i – running the 64-bit version of Microsoft Windows 10 Pro. The system was equipped with an 11th generation Intel Core i5-1145G7 processor operating at 2.60 GHz, featuring 4 physical cores and 8 logical threads. The device was

furnished with 16 GB of physical RAM (random-access memory), of which approximately 15.7 GB were usable for analytical operations. All computations, including clustering and NDVI reconstruction, were performed in local memory without the use of GPU (Graphics Processing Unit) acceleration or parallel computing frameworks.

## RESULTS AND DISCUSSION

Figure 2 presents selected fragments of the orthophoto images in the visible spectrum, acquired for a winter wheat crop on two dates: 28 March and 22 May. The March image reflects an early growth stage (BBCH 29), characterized by low canopy height and limited contrast between the soil surface and vegetation. The soil exhibits a heterogeneous, mosaic-like texture, resulting in areas with varying shades of brown. In the May image (BBCH 55), clearly defined experimental plots are visible, differentiated by vegetation density. Some plots show patches with reduced canopy density, which may indicate biotic stress (e.g., disease) or abiotic stress (e.g., water deficiency).

Prior to applying segmentation algorithms, an analysis of NDVI distribution was conducted for the considered image sections with dimensions of 1200 × 1200 pixels (Figure 3) and selected representative subregions of 200 × 120 pixels (Figure 4). These subregions were chosen to uniformly represent the vegetation state within each acquisition date, allowing for a more accurate assessment of NDVI distribution characteristics. Histogram analysis enabled the evaluation of spatial variability and the overall level of photosynthetic activity in the investigated areas.

The frequency histograms of NDVI values calculated for the images with dimensions of 1200 × 1200 pixels from 28 March and 22 May reveal distinct differences in vegetation status and spatial variability between the two dates (Figure 5). On 28 March, the NDVI values follow a near-normal distribution, with a central tendency around 0.3. The histogram shows a relatively symmetrical spread of values, ranging approximately from −0.1 to 0.7. The mean NDVI value for this date was 0.26, with a standard deviation of 0.16, reflecting a low vegetation cover and a relatively homogeneous field condition, with small differences between the crop and the exposed soil. The presence of pixels with NDVI < 0, albeit limited, indicates bare soil or non-vegetated areas.

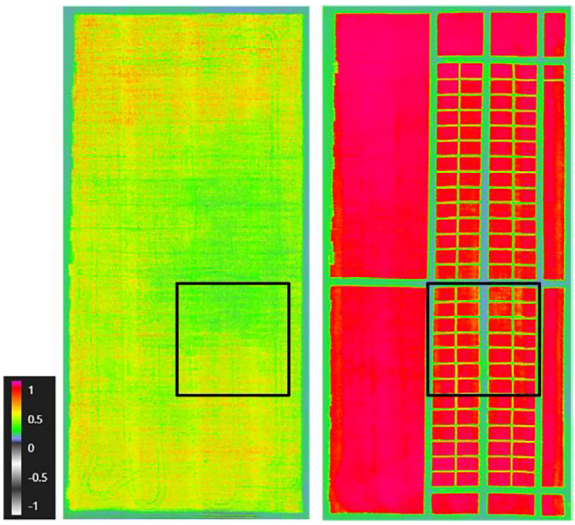


**Figure 3.** NDVI maps of the analyzed winter wheat crop with marked selected areas with dimensions of 1200 × 1200 pixels: 28 March and (b) 22 May

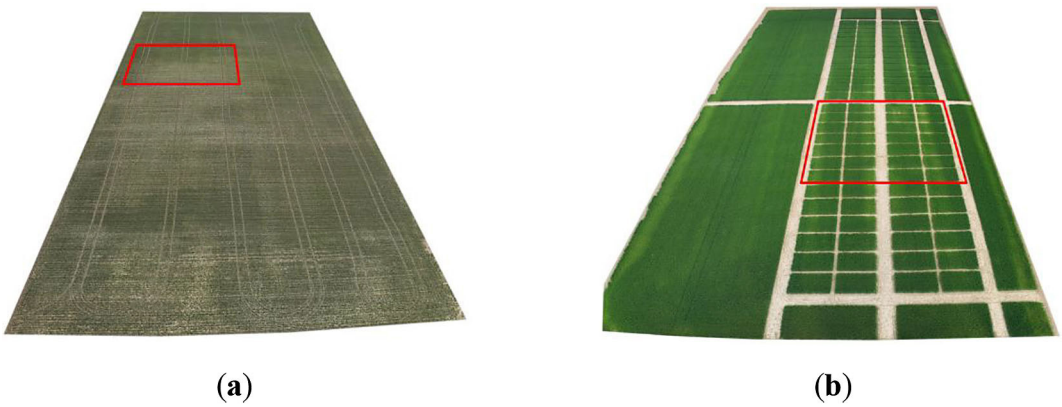


**Figure 2.** RGB image of the analyzed winter wheat crop with marked selected areas with dimensions of 1200 × 1200 pixels: (a) 28 March and (b) 22 May

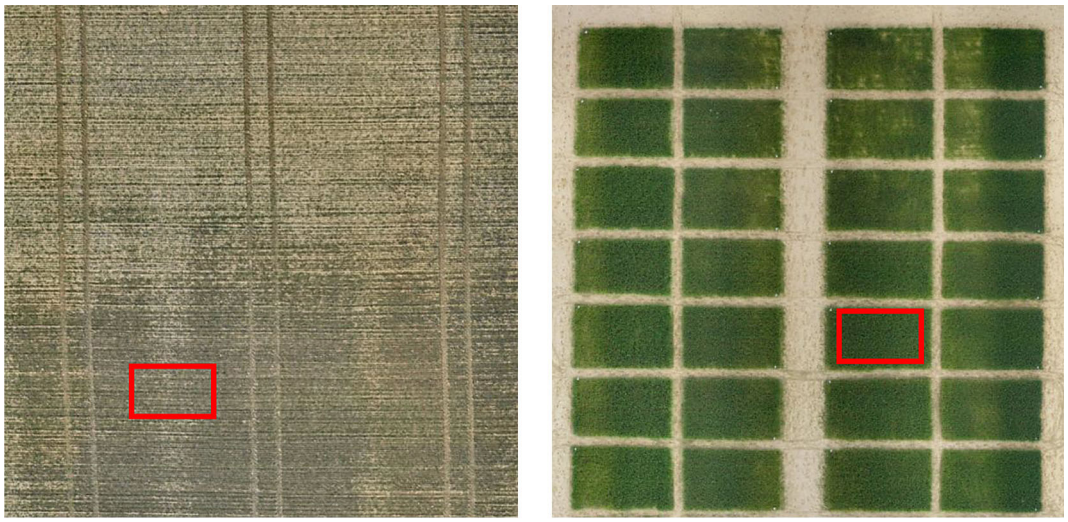

(**a**) (**b**)

**Figure 4.** RGB images of the analyzed winter wheat crop with marked selected areas with dimensions of 200 × 120 pixels for which additional NDVI distribution analysis was conducted: (a) 28 March and (b) 22 May

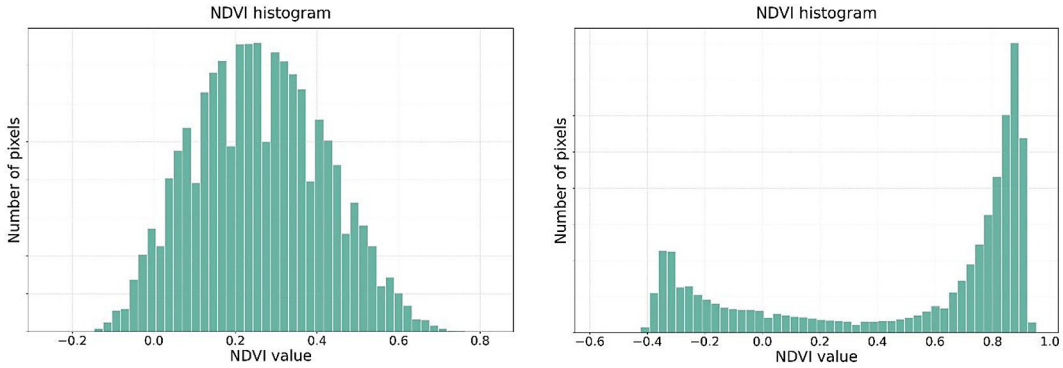


(**a**) (**b**)

**Figure 5.** Histogram of pixel frequency for a given NDVI value for the crop image from: (a) 28 March and (b) 22 May

Conversely, the distribution for 22 May is strongly right-skewed, with a high frequency of NDVI values close to 1.0. The bimodal pattern, with peaks around −0.35 and 0.9, suggests the coexistence of both well-developed vegetation (dense canopy cover) and areas of significantly reduced vegetation or bare soil (e.g., gaps, tramlines, or stressed zones). The mean NDVI for this date increased to 0.48, with a standard deviation of 0.46, indicating a more heterogeneous spatial structure. This is consistent with visual observations of bare soil paths separating individual plots.

To gain more insight into spatial variability within the field, representative subareas (highlighted in red on Figure 4) were analyzed separately. The NDVI histograms for these selected regions are shown in Figure 6.

For 28 March, the histogram retains a unimodal character but is narrower compared to the full-scene distribution. The majority of NDVI values are clustered between 0.2 and 0.6, suggesting greater uniformity within the selected subarea. The central peak around 0.4 confirms moderate vegetative activity, typical for early growth stages (BBCH 29). The mean NDVI value for this region was 0.36, with a standard deviation of 0.14, indicating moderate variability in vegetation cover at this early stage.

In contrast, the histogram for the 22 May subarea is strongly skewed toward higher NDVI values, with a narrow concentration between 0.85 and 0.92. This reflects a nearly complete canopy cover and high photosynthetic activity, consistent with the crop's heading stage (BBCH 55). The

mean NDVI for this subarea reached 0.88, with a standard deviation of just 0.02, confirming that the selected plot was relatively homogeneous in vegetation health, in contrast to more heterogeneous areas seen elsewhere in the image.

These histogram-based observations provide a quantitative basis for assessing crop condition and heterogeneity in both temporal and spatial domains, and they support the application of unsupervised classification algorithms for further segmentation and interpretation of the imagery.

## Analysis of the early growth stage of the crop

This section presents the segmentation analysis of the crop imagery acquired on 28 March, using two unsupervised classification algorithms: K-means and GMM. For each algorithm, two clustering scenarios were considered: 2 clusters and 5 clusters. The selection of these cluster numbers was intended to evaluate the algorithms' ability to identify both dominant vegetation patterns and subtle soil heterogeneity at different segmentation granularities.

Based on the obtained segmentations, corresponding reconstructed NDVI maps were generated to assess the spatial fidelity of vegetation index representation relative to the original imagery. The goal of this stage was to investigate the effectiveness of unsupervised clustering in distinguishing vegetated areas from bare soil during early phenological stages (approximately BBCH 29), where spectral contrast is typically limited. The results are presented in Figure 7–10. A quantitative assessment of segmentation quality and NDVI reconstruction error is discussed in the following sections.

Visual analysis of the segmentation results for both 2 and 5 clusters indicates a high degree of consistency between the compared algorithms (K-means and GMM) in identifying spatial structures. In both cases, the classification primarily captured soil areas with varying contrast, which is directly related to the mosaic-like texture of the soil surface, as observed in the original orthophotos.

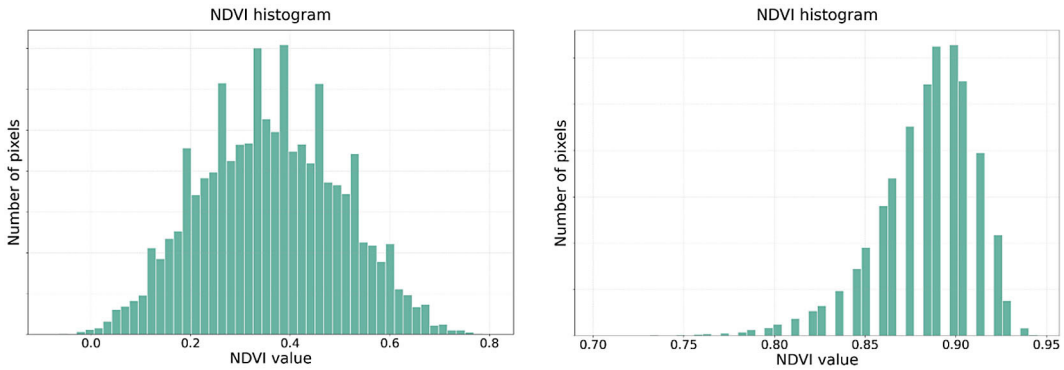


**Figure 6.** Histogram of pixel frequency by NDVI value for the crop image fragment from: (a) 28 March and (b) 22 May

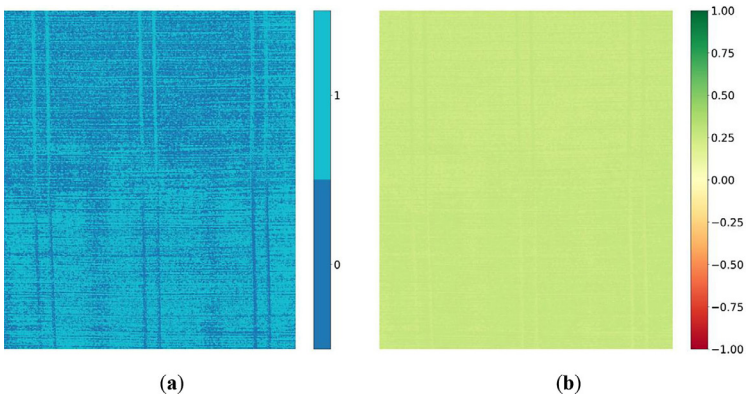


**Figure 7.** (a) Segmentation result using the K-means method and (b) reconstructed NDVI for 2 clusters for the crop from 28 March

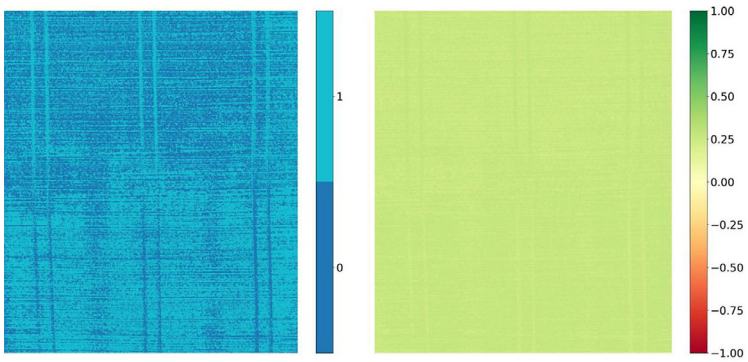


**Figure 8.** (a) Segmentation result using the GMM method and (b) reconstructed NDVI for 2 clusters for the crop from 28 March

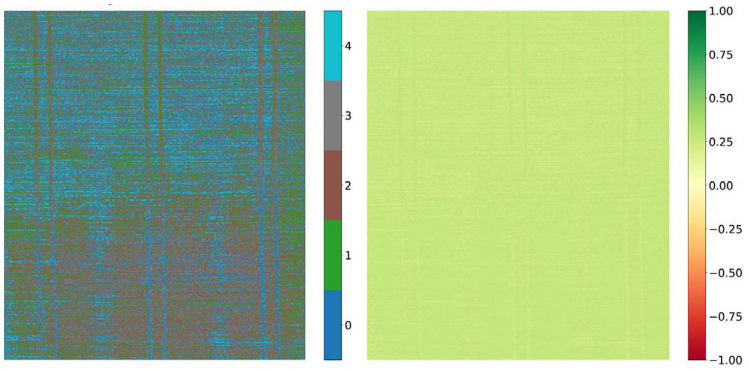


**Figure 9.** (a) Segmentation result using the K-means method and (b) reconstructed NDVI for 5 clusters for the crop from 28 March

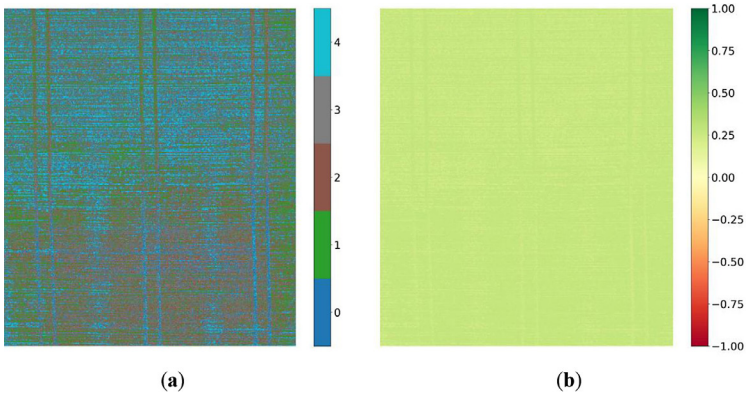


**Figure 10.** (a) Segmentation result using the GMM method and (b) reconstructed NDVI for 5 clusters for the crop from 28 March

For the 28 March scene, in the case of the two-cluster classification, the low height and biomass of the winter wheat plants resulted in weak contrast between vegetation and the soil background. Consequently, vegetated areas were not distinctly delineated by the segmentation algorithms. The resulting image primarily reflected soil heterogeneity rather than the actual spatial distribution of the crop. In contrast, segmentation with five clusters enabled the identification of an additional class (labeled as class no. 4), whose spatial arrangement appeared as

parallel horizontal bands. Initial visual interpretation suggested that this structure might correspond to row-sown plants. However, quantitative analysis confirmed that class 4 exhibited the lowest NDVI values among all clusters. This indicates that these bands represent bare inter-row soil rather than vegetation, despite their regular spacing resembling planted rows. The misinterpretation underscores the challenge of visually differentiating early-stage vegetation from soil patterns in RGB and multispectral imagery when spectral contrast is minimal.

The reconstructed NDVI maps generated based on the assigned clusters exhibited high spatial uniformity. This consistency reflects the robustness of the classification and the relatively low intra-class variability of NDVI values, further supporting the reliability of cluster-based aggregation. Due to the visual similarity of the segmentation results and the limited spatial differentiation, meaningful quantitative interpretation became feasible only after tabulating the output metrics. This enabled objective comparison between the two classification methods and highlighted subtle differences in cluster behavior and spectral properties.

Despite accurately delineating soil structures, segmentation of the scene from the early crop development stage revealed significant limitations. A key constraint is the low radiometric contrast between emerging vegetation and bare soil. During sparse canopy conditions, the spectral signal in NDVI-related bands is often dominated by soil reflectance, affecting the precise identification of vegetative areas. Moreover, spatial heterogeneity in soil texture, the presence of crop residues, and potential shadowing effects may contribute to misclassification, especially in unsupervised methods relying solely on pixel-level spectral features.

From a practical standpoint, the results suggest that the application of unsupervised segmentation algorithms at very early phenological stages (e.g., BBCH 29) provides limited diagnostic value for crop monitoring. Nonetheless, even partial identification of potential vegetation zones – such as indirect delineation of inter-row structures – can offer a starting point for subsequent temporal analyses. These results highlight the potential for early anomaly detection, particularly when segmentation is supported by higher-resolution imagery, ground truth data, or advanced algorithms capable of capturing subtle spectral variations.

For the segmentation with two clusters, both the K-means and GMM algorithms produced nearly identical results (Table 3). Cluster 0 encompassed approximately 43% of the area with an average NDVI of 0.23, while Cluster 1 covered around 57% of the area with a slightly higher NDVI of 0.28. The consistency in both area proportion and NDVI values between the two methods suggests a high degree of agreement in class separation. These values reflect the clear dichotomy between lower- and higher-reflectance regions, which is typical in scenes with dominant soil background and limited vegetative cover.

In the five-cluster segmentation, more nuanced differences between clusters emerged, revealing a slightly more complex spatial structure. For K-means, Cluster 2 (27%) and Cluster 3 (27%) constituted the majority of the area, both exhibiting moderately elevated NDVI values (0.29 and 0.27, respectively), while Cluster 4 (11%) had the lowest NDVI (0.21), potentially indicating

**Table 3.** Percentage shares of the area and the corresponding average NDVI values depending on the number of clusters obtained by the K-means and GMM methods for the crop from 28 March

| K-means | | | GMM | | |
|---|---|---|---|---|---|
| Cluster number | Percentage [%] | Average NDVI [-] | Cluster number | Percentage [%] | Average NDVI [-] |
| 0 | 42.82 | 0.23 | 0 | 42.70 | 0.23 |
| 1 | 57.18 | 0.28 | 1 | 57.30 | 0.28 |
| K-means | | | GMM | | |
| Cluster number | Percentage [%] | Average NDVI [-] | Cluster number | Percentage [%] | Average NDVI [-] |
| 0 | 20.01 | 0.23 | 0 | 19.51 | 0.23 |
| 1 | 14.64 | 0.27 | 1 | 16.84 | 0.27 |
| 2 | 27.10 | 0.29 | 2 | 25.05 | 0.29 |
| 3 | 26.85 | 0.27 | 3 | 25.04 | 0.27 |
| 4 | 11.39 | 0.21 | 4 | 13.55 | 0.21 |

bare soil or non-vegetated areas. Similar trends were observed in the GMM results, with Cluster 4 (14%) also showing the lowest NDVI and Clusters 2 and 3 covering comparable spatial extents (25.05% and 25.04%, respectively).

Overall, both algorithms demonstrated a consistent ability to delineate areas with distinct NDVI magnitudes, particularly in the five-cluster configuration. The relatively small differences in NDVI values and area proportions between corresponding clusters confirm the robustness of the segmentation output across different clustering methods. Notably, Cluster 4, which exhibited the lowest NDVI values and a distinctive strip-like spatial pattern, was initially interpreted as corresponding to early-stage vegetation rows. However, subsequent quantitative analysis revealed that this class more likely represents bare inter-row soil. This correction underscores the need for caution when interpreting segmentation results at early phenological stages, especially in the presence of soil patterns that may mimic vegetative structures in low-resolution or low-contrast imagery.

The analysis of the crop images from 28 March indicates that varying the number of clusters between 2 and 16 did not significantly affect the fit quality of the K-means and GMM models, as measured by MAE, MSE, and $R^2$ metrics. All MAE values hovered around 0.13, while the MSE ranged approximately between 0.02 and 0.03. The coefficient of determination $R^2$ remained low, not exceeding 0.07, regardless of the number of clusters. This suggests a limited ability of the models to explain data variability, which may be due either to inherent limitations of the methods in the context of the analyzed crop or to the low spatial complexity of the data.

An interesting observation concerns the computation times. For the K-means method, the analysis time increased with the number of clusters – from 0.49 seconds for 2 clusters to 3.23 seconds for 16 clusters. Conversely, the GMM model showed a general decreasing trend in analysis time decreased as the number of clusters increased, from 41.09 seconds with 2 clusters to 30.30 seconds with 16 clusters. Importantly, K-means was approximately ten times faster than GMM for the size of the analyzed dataset. It can be hypothesized that, with more clusters, the Gaussian components in the GMM model are more localized, which may reduce the number of iterations needed for convergence, despite the overall higher complexity compared to K-means.

### Analysis of the crop with delineated plots

This section presents the segmentation analysis of the crop imagery acquired on 22 May, focusing on a field with clearly delineated experimental plots of winter wheat surrounded by bare soil. The same two unsupervised classification algorithms used in the previous analysis – K-means and GMM – were applied, with clustering scenarios of 2 and 5 clusters, to maintain consistency in evaluating segmentation performance across different datasets.

The crop was at approximately BBCH 55 growth stage, representing a more advanced phenological phase with well-developed vegetation and clearer spectral contrast between vegetated plots and bare soil. Reconstructed NDVI maps based on the segmentation results were generated for each clustering configuration to assess the spatial accuracy of vegetation index representation relative to the original imagery.

This dataset offers a valuable opportunity to evaluate the effectiveness of unsupervised clustering methods in distinguishing vegetated areas from bare soil under conditions of higher spectral contrast. The segmentation results are presented in Figure 11–14. A detailed quantitative assessment of segmentation quality and NDVI reconstruction error is discussed in the following sections. Segmentation results for the crop imagery acquired on 22 May demonstrate a pattern similar to that observed for the 28 March dataset. The outcomes produced by both K-means and GMM were highly consistent, confirming the robustness of both unsupervised algorithms across different phenological stages.

A key distinction, however, emerged regarding the impact of cluster count. Even with only two clusters, the segmentation successfully differentiated the cultivated plots from the surrounding bare soil. However, this binary classification did not allow for the identification of intra-plot variability. In contrast, the five-cluster segmentation revealed more detailed spatial patterns, enabling the distinction of sub-areas with varying vegetation conditions.

For instance, some experimental plots exhibited patterns assigned to Cluster 0, corresponding to regions with bare soil exposure due to reduced plant density or poor emergence. Cluster 3 was associated with plots showing lighter green vegetation, potentially indicating localized growth stress or nutrient deficiencies. Conversely, areas classified under Cluster 2 represented zones with healthy and dense vegetation cover. Bare soil was mainly

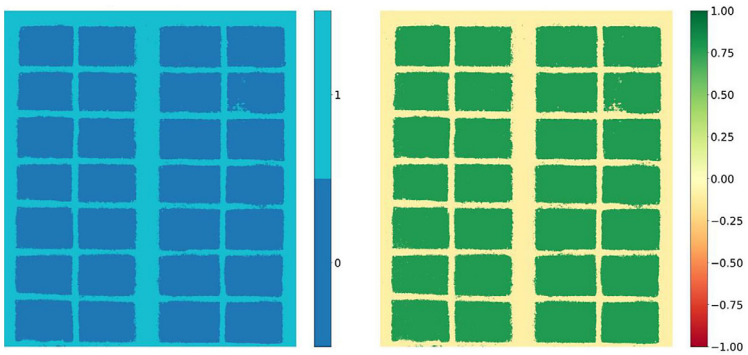


(a) (b)

**Figure 11.** (a) Segmentation result using the K-means method and (b) reconstructed NDVI for 2 clusters for the crop from 22 May

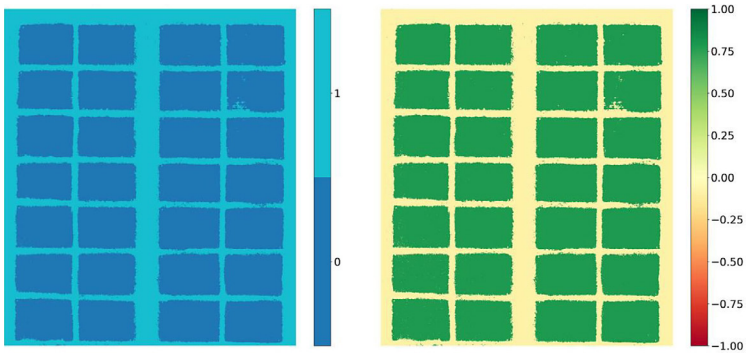


(a) (b)

**Figure 12.** (a) Segmentation result using the GMM method and (b) reconstructed NDVI for 2 clusters for the crop from 22 May

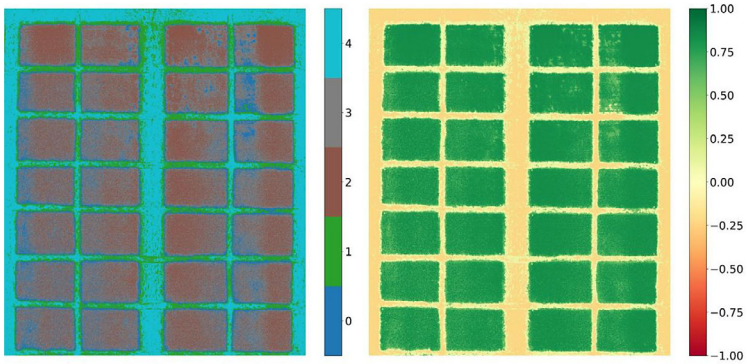


(a) (b)

**Figure 13.** (a) Segmentation result using the K-means method and (b) reconstructed NDVI for 5 clusters for the crop from 22 May

categorized as Clusters 1 and 4, where Cluster 1 typically corresponded to disturbed soil – possibly caused by machinery passes or human activity – while Cluster 4 represented undisturbed soil surfaces. These findings are reflected in the reconstructed NDVI maps derived from the segmentation results. Areas of healthy vegetation showed high NDVI values of approximately 0.9, while stressed vegetation zones exhibited moderate values around 0.6. Bare soil areas were characterized by NDVI values near –0.2, confirming the spectral distinction captured through clustering. In the two-cluster configuration, both K-means and GMM produced nearly identical outcomes (Table 4).

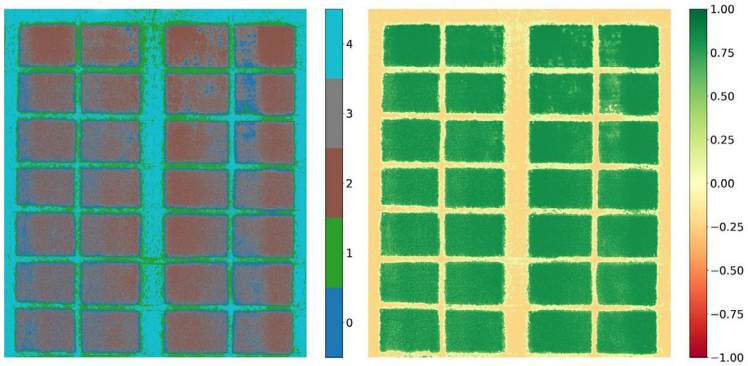


**Figure 14.** (a) Segmentation result using the GMM method and (b) reconstructed NDVI for 5 clusters for the crop from 22 May

Cluster 0, covering about 66% of the image, represented vegetated areas with an average NDVI of 0.78. Cluster 1 covered the remaining 34% and corresponded to bare soil, with an average NDVI of –0.09. The minimal difference in area share and NDVI values between the two algorithms highlights their consistent performance in distinguishing between vegetative cover and non-vegetated ground at a coarse level of segmentation.

In the five-cluster configuration, the segmentation outputs revealed a more nuanced distribution of vegetation conditions. Clusters 2 and 3, with NDVI values of approximately 0.84 and 0.79 respectively, occupied over 54% of the image area and likely correspond to regions with healthy and dense vegetation. Cluster 0 (around 13%) had an intermediate NDVI of 0.62–0.63, potentially indicating stressed or sparse vegetation. Cluster 1 (13%) showed a low NDVI of 0.09, which may suggest soil with plant residues or very early growth. Cluster 4, with the lowest NDVI of –0.23 and covering nearly 20%, clearly represents bare, undisturbed soil.

The consistency between the two algorithms is again evident in the five-cluster results, with all cluster percentages and mean NDVI values differing by no more than ±1.2% or ±0.01, reinforcing the robustness of the segmentation methodology.

In the case of the crop analysis from 22 May, changing the number of clusters from 2 to 16 did not significantly affect the fitting quality of the K-means and GMM models, as evaluated by MAE, MSE, and the coefficient of determination $R^2$. The MAE values ranged from 0.11 to 0.15, while MSE fluctuated between 0.03 and 0.05. The $R^2$ coefficient remained high, from 0.78 to 0.86, indicating a good ability of both models to explain data variability in this case. The high $R^2$ values may result from the distinct spatial structure of the experimental plots and greater heterogeneity of vegetation, which facilitates segmentation and classification based on vegetation indices.

**Table 4.** Percentage shares of the area and the corresponding average NDVI values depending on the number of clusters obtained by the K-means and GMM methods for the crop from 22 May

| K-means | | | GMM | | |
|---|---|---|---|---|---|
| Cluster number | Percentage [%] | Average NDVI [-] | Cluster number | Percentage [%] | Average NDVI [-] |
| 0 | 66.01 | 0.78 | 0 | 65.81 | 0.78 |
| 1 | 33.99 | −0.09 | 1 | 34.19 | −0.09 |
| K-means | | | GMM | | |
| Cluster number | Percentage [%] | Average NDVI [-] | Cluster number | Percentage [%] | Average NDVI [-] |
| 0 | 12.73 | 0.62 | 0 | 13.93 | 0.63 |
| 1 | 13.12 | 0.09 | 1 | 13.11 | 0.09 |
| 2 | 23.32 | 0.84 | 2 | 23.18 | 0.84 |
| 3 | 31.05 | 0.79 | 3 | 30.02 | 0.79 |
| 4 | 19.78 | −0.23 | 4 | 19.76 | −0.23 |

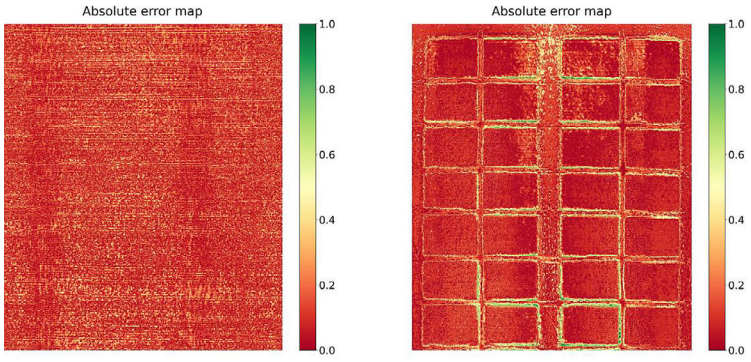


(**a**) (**b**)

**Figure 15.** Example error map for the K-means method with 5 clusters for the crop from: (a) 28 March and (b) 22 May

Regarding computational time, for the K-means method, a systematic increase was observed as the number of clusters grew – from 0.36 s for 2 clusters to 1.78 s for 16 clusters. Conversely, the GMM algorithm's runtime was more variable, ranging from 18.46 to 30.90 seconds, without a clear trend. This variability may stem from differing numbers of iterations required for model convergence at various cluster counts, as well as the influence of parameter initialization on the training process. Nonetheless, K-means proved to be significantly faster than GMM for the analyzed dataset.

Comparing results between the two measurement dates reveals notable differences in algorithm behavior. At the early growth stage (28 March), K-means was nearly ten times faster than GMM, but both models exhibited low segmentation accuracy, likely due to weak spectral separability and low vegetation cover. In contrast, for the later growth stage (22 May), both models achieved high segmentation accuracy. K-means remained the faster method, possibly due to the more distinct data structure and stronger clustering tendencies in the NDVI values, which facilitated more efficient grouping.

It is also worth emphasizing that classification stability, measured by the repeatability of algorithm results across multiple runs, remains an important practical factor, especially in precision agriculture applications. Future studies should include multiple algorithm runs and stability assessments to fully evaluate the practical applicability of these methods. Exemplary absolute error maps for the K-means algorithm with five clusters, applied to the imagery from 28 March and 22 May, are presented in Figure 15. In the 28 March image, the error values are distributed in a relatively uniform and random pattern across the scene. In small pixel clusters – likely representing sparse vegetation or soil heterogeneity – the absolute error reached up to 0.35 (normalized units), while the remaining areas showed near-zero error, indicating effective pixel grouping.

In contrast, the 22 May image reveals increased error values along the boundaries of the experimental plots, where the absolute error locally approached 1.0. This increase is attributed to the presence of gradual transitions between adjacent plots with differing vegetation properties, which pose a challenge for algorithms relying on discrete classification boundaries.

Nevertheless, within the core areas of the plots, the number of pixels exhibiting significant error values (above 0.3) remained relatively low. This observation supports the overall accuracy and robustness of the K-means segmentation in distinguishing management zones under conditions of advanced crop development.

## CONCLUSIONS

The article presents a comparison of two popular unsupervised segmentation algorithms (K-means and GMM) in the context of analyzing multispectral drone data acquired over a winter wheat crop. The aim of the study is to evaluate the effectiveness of both methods in spatial differentiation of crop condition. The study showed that the performance and efficiency of the K-means and GMM algorithms are highly dependent on the characteristics of the analyzed data, which vary with the crop's phenological stage. In the early growth stage (28 March), when the spectral

contrast between vegetation and soil was low, both algorithms demonstrated limited ability to explain data variability ($R^2 < 0.07$). Under these conditions, the K-means algorithm was nearly ten times faster than GMM. However, segmentation at this stage has limited diagnostic value for crop monitoring.

Unsupervised segmentation at early crop stages was shown to have limited diagnostic value due to low spectral contrast, whereas at later stages both algorithms reliably captured spatial variability. Although additional temporal acquisitions could enhance early stress detection, the present comparison across across varying conditions provides a clear framework for assessing the practical applicability of K-means and GMM in UAV-based crop monitoring. In the later growth stage (22 May), with a well-defined spatial structure of field plots and high vegetation heterogeneity, both models achieved high goodness-of-fit ($R^2$ ranging from 0.78 to 0.86). Notably, the K-means algorithm remained significantly faster than GMM, confirming its computational advantage across both datasets. The choice of the optimal segmentation algorithm should take into account both the characteristics of the input data and the computational time requirements. From a practical perspective, differences in processing time are substantial. The consistently shorter runtime of K-means may be critical when working with large volumes of drone imagery or in time-sensitive applications. While GMM generally required more time, both algorithms achieved high segmentation accuracy during complex crop stages, such as in May, suggesting their suitability depends more on runtime constraints than on output quality. Therefore, the choice of algorithm should be guided primarily by processing efficiency, as both methods yielded comparable segmentation accuracy in the analyzed datasets.

Unsupervised segmentation can be used for the classification of agricultural areas and for monitoring vegetation changes, such as crop growth or stress response. The results of the analysis can serve as a foundation for developing automated tools to support agronomic decision-making, particularly in the context of precise and sustainable resource management.

## REFERENCES


1. Huang, S., Tang, L., Hupy, J. P., Wang, Y., Shao, G. A commentary review on the use of normalized difference vegetation index (NDVI) in the era of popular remote sensing. Journal of Forestry Research, 2021; 32(1), 1–6. https://doi.org/10.1007/s11676-020-01155-1
2. Karpiński P, Kocira S. Possibilities of using a multispectral camera to assess the effects of biostimulant application in soybean cultivation. Sensors. 2025; 25(11):3464. https://doi.org/10.3390/s25113464
3. Karpiński, P. The Use of Drones in Agriculture: Perspectives and Limitations. In International Symposium on Farm Machinery and Processes Management in Sustainable Agriculture 2024, June; 219–228. Cham: Springer Nature Switzerland. https://doi.org/10.1007/978-3-031-70955-5_24
4. Phang, S. K., Chiang, T. H. A., Happonen, A., Chang, M. M. L. From satellite to UAV-based remote sensing: A review on precision agriculture. Ieee Access, 2023; 11, 127057–127076. https://doi.org/10.1109/ACCESS.2023.3330886
5. Mouret, F., Albughdadi, M., Duthoit, S., Kouamé, D., Rieu, G., Tourneret, J. Y. Reconstruction of Sentinel-2 derived time series using robust Gaussian mixture models —Application to the detection of anomalous crop development. Computers and Electronics in Agriculture, 2022; 198, 106983. https://doi.org/10.1016/j.compag.2022.106983
6. Othman, K., Mohd, M. N., Rahman, M. Q. A., Nor, M. H. M., Ngadimon, K., Sulaiman, Z. A Mixed Gaussian Distribution Approach using the Expectation-Maximization Algorithm for Topography Predictive Modelling. WSEAS Transactions on Computers, 2025; 24, 29–41. https://doi.org/10.37394/23205.2025.24.4
7. Peng, L., Xin, H. N., Lv, C. X., Li, N., Li, Y. F., Geng, Q. L.,..., Lai, N. Inversion of nitrogen and phosphorus contents in cotton leaves based on the Gaussian mixture model and differences in hyperspectral features of UAV. Spectrochimica Acta Part A: Molecular and Biomolecular Spectroscopy, 2024; 125419. https://doi.org/10.1016/j.saa.2024.125419
8. Rajesh, D. Application of spatial data mining for agriculture. International Journal of Computer Applications, 2011; 15(2), 7–9. https://doi.org/10.5120/1922-2566
9. Zhang, X., Wu, S., Yan, X., Chen, Z. A global classification of vegetation based on NDVI, rainfall and temperature. International Journal of Climatology, 2017; 37(5), 2318–2324. https://doi.org/10.1002/joc.4847
10. Mucherino, A., Papajorgji, P., Pardalos, P. M. A survey of data mining techniques applied to agriculture. Operational Research, 2009; 9, 121–140. https://doi.org/10.1007/s12351-009-0054-6
11. Vandana, B., Kumar, S. Hybrid K mean clustering algorithm for crop production analysis in agriculture. Int J Inno Techn Explo Eng, 2019; 9(2S), 9–12. https://doi.org/10.35940/ijitee.B1002.1292S19
12. Zhang, Y., Li, L., Chun, C., Wen, Y., Li, C., Xu,

G. Data-driven Bayesian Gaussian mixture optimized anchor box model for accurate and efficient detection of green citrus. Computers and Electronics in Agriculture, 2024; 225, 109366. https://doi.org/10.1016/j.compag.2024.109366

13. Li, C., Niu, B. Design of smart agriculture based on big data and Internet of things. International Journal of Distributed Sensor Networks, 2020; 16(5), 1550147720917065. https://doi.org/10.1177/1550147720917065
14. Geetha, M. C. S. A survey on data mining techniques in agriculture. International journal of innovative research in computer and communication engineering, 2015; 3(2), 887–892. https://doi.org/10.15680/ijircce.2015.0302071
15. Kaur, M., Gulati, H., Kundra, H. Data mining in agriculture on crop price prediction: techniques and applications. International Journal of Computer Applications, 2014; 99(12), 1–3. https://doi.org/10.5120/17422-8273
16. Majumdar, J., Naraseeyappa, S., Ankalaki, S. Analysis of agriculture data using data mining techniques: application of big data. Journal of Big data, 2017; 4(1), 20. https://doi.org/10.1186/s40537-017-0077-4
17. Yadav, S. A., Sahoo, B. M., Sharma, S., Das, L. An analysis of data mining techniques to analyze the effect of weather on agriculture. In 2020 international conference on intelligent engineering and management (ICIEM). 2020, June; 29–32. IEEE. https://doi.org/10.1109/ICIEM48762.2020.9160110
18. Kuricheti, G., Supriya, P. Computer vision based turmeric leaf disease detection and classification: a step to smart agriculture. In 2019 3rd International Conference on Trends in Electronics and Informatics (ICOEI). 2019, April; 545–549. IEEE. https://doi.org/10.1109/ICOEI.2019.8862706
19. Ribeiro Junior, F. M., Bianchi, R. A., Prati, R. C., Kolehmainen, K., Soininen, J. P., Kamienski, C. A. Data reduction based on machine learning algorithms for fog computing in IoT smart agriculture. Biosystems Engineering, 2022; 223, 142–158. https://doi.org/10.1016/j.biosystemseng.2021.12.021
20. Ge, L., Yang, Z., Sun, Z., Zhang, G., Zhang, M., Zhang, K.,..., Li, W. A method for broccoli seedling recognition in natural environment based on binocular stereo vision and Gaussian mixture model. Sensors, 2019; 19(5), 1132. https://doi.org/10.3390/s19051132
21. Kim, B. H., Kwon, H., Kim, W. Deciphering individual triticale grain weight patterns: A gaussian mixture model approach. PloS one, 2024; 19(11), e0313942. https://doi.org/10.1371/journal.pone.0313942
22. Tian, K., Li, J., Zeng, J., Evans, A., Zhang, L. Segmentation of tomato leaf images based on adaptive clustering number of K-means algorithm. Computers and Electronics in Agriculture, 2019; 165, 104962. https://doi.org/10.1016/j.compag.2019.104962
23. Yu, Y., Velastin, S. A., Yin, F. Automatic grading of apples based on multi-features and weighted K-means clustering algorithm. Information processing in agriculture, 2020; 7(4), 556–565. https://doi.org/10.1016/j.inpa.2019.11.003
24. Sodjinou, S. G., Mohammadi, V., Mahama, A. T. S., Gouton, P. A deep semantic segmentation-based algorithm to segment crops and weeds in agronomic color images. information processing in agriculture, 2022; 9(3), 355–364. https://doi.org/10.1016/j.inpa.2021.08.003
25. Tang, J., Wang, D., Zhang, Z., He, L., Xin, J., Xu, Y. Weed identification based on K-means feature learning combined with convolutional neural network. Computers and electronics in agriculture, 2017; 135, 63–70. https://doi.org/10.1016/j.compag.2017.01.001
26. Valicharla, S. K., Wang, J., Li, X., Gururajan, S., Karimzadeh, R., Park, Y. L. Morning glory flower detection in aerial images using semi-supervised segmentation with gaussian mixture models. AgriEngineering, 2024; 6(1), 555–573. https://doi.org/10.3390/agriengineering6010034
27. Mazzia, V., Comba, L., Khaliq, A., Chiaberge, M., Gay, P. UAV and machine learning based refinement of a satellite-driven vegetation index for precision agriculture. Sensors, 2020; 20(9), 2530. https://doi.org/110.3390/s20092530
28. Aqel, D., Al-Zubi, S., Mughaid, A., Jararweh, Y. Extreme learning machine for plant diseases classification: a sustainable approach for smart agriculture. Cluster Computing, 2022; 25(3), 2007–2020. https://doi.org/10.1007/s10586-021-03397-y
29. Kuricheti, G., Supriya, P. Computer vision based turmeric leaf disease detection and classification: a step to smart agriculture. In 2019 3rd International Conference on Trends in Electronics and Informatics (ICOEI). 2019, April; 545–549. IEEE. https://doi.org/10.1109/ICOEI.2019.8862706
30. Brubeck-Hernandez, F., Vladimirova, T., Pooley, M., Thompson, R., Knight, B. Zone management in precision agriculture using satellite imagery. In 2019 NASA/ESA Conference on Adaptive Hardware and Systems (AHS). 2019, July; 65–71. IEEE. https://doi.org/10.1109/AHS.2019.00006
31. Di, X., Wang, X. Method for Zoning Corn Based on the NDVI and the Improved SOM-K-Means Algorithm. Journal of the ASABE, 2023; 66(4), 943–953. https://doi.org/10.13031/ja.15081
32. Nugumanova, A., Maulit, A., Sutula, M. Clustering Analysis Applied to NDVI Maps to Delimit Management Zones for Grain Crops. In Asian Conference on Intelligent Information and Database Systems 2022, November; 445–457. Cham: Springer Nature Switzerland. https://doi.org/10.1007/978-3-031-21967-2_36

33. Gavioli, A., de Souza, E. G., Bazzi, C. L., Schenatto, K., Betzek, N. M. Identification of management zones in precision agriculture: An evaluation of alternative cluster analysis methods. Biosystems engineering, 2019; 181, 86–102. https://doi.org/10.1016/j.biosystemseng.2019.02.019
34. Javadi, S. H., Guerrero, A., Mouazen, A. M. Clustering and smoothing pipeline for management zone delineation using proximal and remote sensing. Sensors, 2022; 22(2), 645. https://doi.org/10.3390/s22020645
35. Johann, J.A. Rocham, J.V., Oliveira, S.R.M., Rodrigues, L.H.A., Lamparelli, R.A.C. Data mining techniques for identification of spectrally homogeneous areas using NDVI temporal profiles of soybean crop, Engenharia Agrícola, 2013; 33(3), 511–524. https://doi.org/10.1590/S0100-69162013000300008
36. Ahmed, K. R., Akter, S. Analysis of landcover change in southwest Bengal delta due to floods by NDVI, NDWI and K-means cluster with landsat multi-spectral surface reflectance satellite data. Remote Sensing Applications: Society and Environment, 2017; 8, 168–181. https://doi.org/10.1016/j.rsase.2017.08.010
37. Iryanti, M., Nurjanah, R., Arifin, M. Landslide mapping using K-Means cluster by NDVI data in Garut, West Java, Indonesia. In Journal of Physics: Conference Series 2024, November; 2900(1), 012020). IOP Publishing. https://doi.org/10.1088/1742-6596/2900/1/012020
38. Guan, H., Huang, J., Li, L., Li, X., Miao, S., Su, W.,..., Huang, H. Improved Gaussian mixture model to map the flooded crops of VV and VH polarization data. Remote Sensing of Environment, 2023; 295, 113714. https://doi.org/10.1016/j.rse.2023.113714
39. Sanz, E., Sotoca, J. J. M., Saa-Requejo, A., Díaz-Ambrona, C. H., Ruiz-Ramos, M., Rodríguez, A., Tarquis, A. M. Clustering arid rangelands based on NDVI annual patterns and their persistence. Remote Sensing, 2022; 14(19), 4949. https://doi.org/10.3390/rs14194949
40. Lemenkova, P., Debeir, O. (2022). R Libraries for remote sensing data classification by K-means clustering and NDVI computation in Congo River Basin, DRC. Applied Sciences, 12(24), 12554. https://doi.org/10.3390/app122412554
41. Skakun, S., Franch, B., Vermote, E., Roger, J. C., Becker-Reshef, I., Justice, C., Kussul, N. Early season large-area winter crop mapping using MODIS NDVI data, growing degree days information and a Gaussian mixture model. Remote Sensing of Environment, 2017; 195, 244–258. https://doi.org/10.1016/j.rse.2017.04.026
42. Xiao, G., Du, K., Miao, S., Li, X., Gobin, A., Bai, T.,..., Huang, J. Improved soybean mapping with spectral Gaussian mixture modeling. Journal of Remote Sensing, 2025; 5, 0473. https://doi.org/10.34133/remotesensing.0473
43. Liyantono, Almadani, Y., Adillah, Y., Yusuf, M. M., Mahbub, M. N. R., & Fatikhunnada, A. Analysis of paddy productivity using NDVI and K-means clustering in Cibarusah Jaya, Bekasi Regency. In IOP conference series: materials science and engineering 2019, June; 557(1), 012085. IOP Publishing. https://doi.org/10.1088/1757-899X/557/1/012085
44. Naser, M. A., Khosla, R., Longchamps, L., Dahal, S. Using NDVI to differentiate wheat genotypes productivity under dryland and irrigated conditions. Remote Sensing, 2020; 12(5), 824. https://doi.org/10.3390/rs12050824
45. Zhu, C., Ding, J., Zhang, Z., Wang, J., Wang, Z., Chen, X., Wang, J. SPAD monitoring of saline vegetation based on Gaussian mixture model and UAV hyperspectral image feature classification. Computers and Electronics in Agriculture, 2022; 200, 107236. https://doi.org/10.1016/j.compag.2022.107236
46. Awon, O., and Goswami, M. Synergizing random forest and k means algorithms: an analytical study for precise crop recommendation in southeast Asia. Asian Journal of Research in Computer Science 2024; 17(8):5 8–69. https://doi.org/10.9734/ajrcos/2024/v17i7490
47. Nikhar, M., Thakre, L. P. Smart agricultural farm enhancement with k-means learning. In International Journal of Innovative Technology and Exploring Engineering (IJITEE) 2020; 9(8), 166–170. https://doi.org/10.35940/ijitee.H6222.069820
48. Vitharana, U. W., Van Meirvenne, M., Simpson, D., Cockx, L., De Baerdemaeker, J. Key soil and topographic properties to delineate potential management classes for precision agriculture in the European loess area. Geoderma, 2008; 143(1–2), 206–215. https://doi.org/10.1016/j.geoderma.2007.11.003
49. Jebarani, P. E., Umadevi, N., Dang, H., Pomplun, M. A novel hybrid K-means and GMM machine learning model for breast cancer detection. IEEE Access, 2021; 9, 146153–146162. https://doi.org/10.1109/ACCESS.2021.3123425
50. Wang, Z., Da Cunha, C., Ritou, M., Furet, B. Comparison of K-means and GMM methods for contextual clustering in HSM. Procedia Manufacturing, 2019; 28, 154–159. https://doi.org/10.1016/j.promfg.2018.12.025
51. El Mohtadi, R., Rzeczkowski, J., Korzec-Strzałka, I., Samborski, S., Aymerich, F., Czajka, A. Experimental tensile testing of the lap joint composite laminates supported with the acoustic emission and machine learning techniques. Composite Structures, 2024; 345, 118394. https://doi.org/10.1016/j.compstruct.2024.118394
52. Kong, C., Khalid, H., Gao, Z. Construction of agricultural product consumer group portrait and analysis of precision marketing strategies based on K-means cluster analysis, Journal of Autonomous Intelligence, 2024; 7(1), 1–8. https://doi.org/10.32629/jai.v7i1.903